ChemPubSoc Europe

DOI: 10.1002/cphc.201501129

CHEMPHYSCHEM Articles

Label-Free Fluctuation Spectroscopy Based on Coherent Anti-Stokes Raman Scattering from Bulk Water Molecules

M. D. Rabasovic[+],[a, b] E. Sisamakis[+],[a, d] S. Wennmalm,*[c] and J. Widengren*[a]

Nanoparticles (NPs) and molecules can be analyzed by inverse fluorescence correlation spectroscopy (iFCS) as they pass through an open detection volume, displacing fractions of the fluorescence-emitting solution in which they are dissolved. iFCS does not require the NPs or molecules to be labeled. However, fluorophores in μM–mM concentrations are needed for the solution signal. Here, we instead use coherent anti-Stokes Raman scattering (CARS) from plain water molecules as the signal from the solution. By this fully label-free approach, termed inverse CARS-based correlation spectroscopy (iCARS-CS), NPs that are a few tenths of nm in diameter and at pM concentrations can be analyzed, and their absolute volumes/concentrations can be determined. Likewise, lipid vesicles can be analyzed as they diffuse/flow through the detection volume by using CARS fluctuations from the surrounding water molecules. iCARS–CS could likely offer a broadly applicable, label-free characterization technique of, for example, NPs, small lipid exosomes, or microparticles in biomolecular diagnostics and screening, and can also utilize CARS signals from biologically relevant media other than water.

1. Introduction

By using fluorescence correlation spectroscopy (FCS), information about sparse amounts of fluorescent molecules can be obtained through fluctuations in the detected fluorescence intensity.[1,2] The ability to quickly and noninvasively determine the concentrations and sizes of the molecules and to characterize the reactions and dynamic processes in which they are involved, has made FCS a widely used tool for biomolecular analysis in solutions as well as in living cells (see Refs. [3–5] for reviews). In FCS measurements, the molecules under study must be intrinsically fluorescent or fluorescently labeled, and need to fluoresce brightly and have high photostability.[6] Alternatively, in the recently developed technique inverse FCS (iFCS), the fluorescence signal from the medium surrounding the molecules/particles is analyzed rather than the fluorescence signal from the molecules/particles themselves.[7,8] By the addition of μM–mM concentrations of fluorophores to the surrounding medium, unlabeled nanoparticles (NPs) generate negative spikes in the signal as they diffuse through the detection volume. In contrast to FCS, the added fluorophores in the iFCS experiments need not be highly fluorescent and photostable. A fairly broad range of fluorophores can be used, as long as they provide a specific signal that reflects the extent to which the solution is displaced by particles in the detection volume. The depth of the negative spikes, retrieved from the intensity distribution or auto- or cross-correlation analysis of the detected fluorescence intensity, gives a direct measure of the absolute volume of the NPs.[7–9] This provides a more sensitive estimation of the molecular size than the diffusion coefficient obtained from FCS measurements, which scales only with the cubic root of the particle mass.[10]

Recent extensions of iFCS include inverse fluorescence cross-correlation spectroscopy (iFCCS),[9] in which the fluorescence signal from labeled particles/biomolecules is cross-correlated with the signal from their surrounding fluorescent medium. iFCCS simplifies the direct estimation of the absolute particle volume, and by simultaneous analysis of labeled and unlabeled particles the degree of labeling can be determined. Furthermore, by reducing the volume observed for iFCS measurements, for example, by confinement of the detection to sub-wavelength gold film apertures,[11] smaller NPs and even proteins can be analyzed. By extending the concept to raster scanning imaging (scanning inverse FCS; siFCS), the absolute sizes

[a] Dr. M. D. Rabasovic,[+] Dr. E. Sisamakis,[+] Dr. J. Widengren
Dept. Exp. Biomolecular Physics/Applied Physics
Royal Institute of Technology-KTH, Albanova University Center
10691 Stockholm (Sweden)
E-mail: jwideng@kth.se

[b] Dr. M. D. Rabasovic[+]
Institute of Physics, University of Belgrade
Pregrevica 118, 11080 Belgrade-Zemun (Serbia)

[c] Dr. S. Wennmalm
Dept. Exp. Biomolecular Physics/Applied Physics
Royal Institute of Technology-KTH, Science for Life Laboratory
17165 Solna (Sweden)
E-mail: stewen@kth.se

[d] Dr. E. Sisamakis[+]
Current address:
PicoQuant GmbH, RudowerChaussee 29
12489 Berlin (Germany)

[+] These authors contributed equally to the work

Supporting Information and ORCID(s) from the author(s) for this article are available on the WWW under http://dx.doi.org/10.1002/cphc.201501129.

of nanodomains and possibly protein clusters in cell membranes can also be determined.[12]

Although there is no requirement that the particles under study are labeled for iFCS, organic fluorophores must be added to the surrounding medium. A feature that iFCS shares with FCS is, thus, that it requires some kind of labeling. So far dye solutions in the μM up to 2 mM range have been used for analyses of 3D diffusion,[7–9,11] and for 2D membrane analyses, lipid dyes have been used at a partition coefficient between 1:2000 and 1:100.[12]

In this study, we present a technique that overcomes the need for fluorophores for such measurements. We show that a specific signal, which is inherent to the molecules of the surrounding medium (aqueous solution), is offered by coherent anti-Stokes Raman scattering (CARS) from the plain medium (water) molecules themselves. This signal has the necessary selectivity and signal strength to serve as a label-free alternative to fluorescence from dissolved fluorophores in iFCS.

With regards to other label-free correlation spectroscopy techniques, dynamic light scattering (DLS)[13] is the most extensively used and can be used to derive the size of moving particles from their diffusion coefficients. However, our approach provides, like iFCS, a direct, more-sensitive measure of particle sizes from the depth of the negative spikes in the signal of the studied solution. This possibility can, for example, be used in microfluidic flow measurements, where diffusion coefficients cannot be estimated. Moreover, in contrast to our approach, DLS cannot determine particle concentrations, cannot be easily combined with fluorescence readouts, and does not lend itself to detection in highly confined detection volumes with subsequent imaging/scanning capabilities. Correlation spectroscopies with confined detection volumes, with readouts that can replace the fluorescence signal used in FCS, have also been successfully demonstrated, based on surface-enhanced resonance Raman scattering (SERRS),[14,15] resonance light scattering,[16] nonlinear light scattering,[17] plasmon luminescence,[18] coherent anti-Stokes Raman scattering (CARS),[19,20] photothermal interferometric,[21] and other interferometric readouts.[22,23] Some of these readouts can also be considered to be label free. However, for all these readout modalities, the signal originates from the particles studied, not from the surrounding medium. In FCS, the fluorescence brightness of the individual molecules/particles studied is a key figure of merit.[24] Likewise, the signal per particle/molecule of these other read-out modalities[13–23] needs to be in parity with the fluorescence signal they replace. This requirement regarding molecular/particle brightness restricts the range of molecules/particles that can be studied with these spectroscopic approaches. In contrast, the CARS signal retrieved from individual water molecules in our approach is weak. However, the overall signal is sufficient, given the high concentration of water molecules in aqueous solutions, and the fact that CARS is a coherent process that is amplified nonlinearly with the concentration of active scatterers in the medium. The signal is sufficient to readily allow the specific analysis of the displacement dynamics of small volumes of water, as a consequence of the movement of particles into and out of a confined detection volume. By our approach, which we have named CARS-based inverse correlation spectroscopy (iCARS-CS), correlation analysis of the intensity time traces of the CARS signal allowed the sizes of polystyrene beads having diameters ranging from 1 μm down to less than 100 nm to be determined in the detection volumes. We also demonstrate that iCARS-CS curves can be used to detect lipid vesicles. Given the wide use of NPs in biomolecular diagnostics and screening, and the increasingly recognized role of small lipid vesicles, so-called exosomes and microparticles, in biology and medicine,[25–28] we believe that iCARS-CS can offer an interesting label-free technique in these fields of research.

2. Results and Discussion

2.1. Validation of the Basic Concept

The basic concept of iCARS-CS is illustrated in Figure 1. In the aqueous solution under study, a CARS signal can be generated in the spatially and temporally overlapping foci of two femtosecond laser beams with a difference in their optical frequencies that corresponds to the 3100–3600 cm^{-1} Raman band of the water molecules (Figure 1 A). When the volume of the overlapping laser foci (the detection volume) is void of particles it is entirely filled up by water molecules, and a CARS signal is predominantly emitted in the forward direction (Figure 1 B).[20,29,30] As a particle transverses through the volume a negative spike can be observed in the forward CARS intensity time trace for two major reasons (Figure 1 C): 1) The particle displaces water out of the focal volume, thereby reducing the number of molecules from which the CARS signal is generated. 2) Disturbance of the coherence, which results in a change in the angular distribution of the CARS signal.[20,29–31] Owing to the disturbance of the coherence, a backward CARS signal also appears. When the particle exits the focal detection volume, it

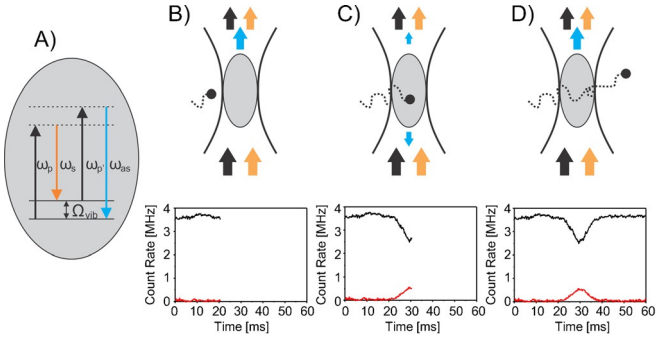

Figure 1. A) When the foci of a pump/probe laser beam with the optical frequency $\omega_p = \omega_{p'}$ (black) and a Stokes laser beam with the frequency ω_s (orange) overlap in space and time, and their frequencies match the Raman band of the water molecules, $\Omega_{vib} = \omega_p - \omega_s$, an anti-Stokes signal (blue) is generated at a frequency of $\omega_{as} = 2\omega_p - \omega_s$ from the water molecules in the volume of focal overlap (gray). B–D) The signals analyzed in iCARS-CS. The upper row illustrates the CARS signals (blue arrows) generated from the water molecules in the focal detection volume, and how it changes upon the transit of a particle through the volume. Black and orange arrows show the Stokes and pump beams. The graphs in the lower row depict the time dependence of the signal in the forward (black curve) and in the backward direction (red curve). See text for further explanations.

will be entirely filled with water molecules again, and the coherence will be restored. The forward signal will then be fully recovered and the backward signal will disappear, (Figure 1 D).

To provide initial experimental evidence that traces of forward and backward CARS signals can be generated and detected as outlined above, latex and silica beads were studied under flow conditions (see the Experimental Section for a description of the setup). Under our conditions, a pump/probe irradiation field at 617 nm and a Stokes irradiation field at 779 nm, which have a frequency difference that matches the Raman band of water at 3100–3600 cm^{-1}, resulted in the strongest specific CARS signal from the water molecules, at a wavelength of 511 nm. With a pump/probe laser beam power of 10 mW and a Stokes beam power of 5 mW, a CARS signal in the range of 1–5 MHz was detected in the forward direction (Figure 2). For particles that are large enough and with their concentrations adjusted such that on average less than one particle resided in the detection volume at the same time, clear negative spikes (dips) were observed in the forward CARS signals (Figure 2). Simultaneous recording the CARS signal in the forward and backward direction then revealed that the positive spikes in the backward direction coincide with the negative spikes in the forward direction. This indicates that the spikes in the forward and backward direction are not random fluctuations, but both originate from the same individual transits of particles through the focal detection volume. The fact that the detected spikes are negative in the forward direction and positive in the backward direction is in contrast to the signal in iFCS, where the spikes (of the fluorescence signal from the bulk) are negative in both the forward and backward directions. In this sense, the backward detected (EPI, i.e. epi-detected, collected by the same objective as used for focusing the pump and probe beams) signal in iCARS-CS is rather analogous to the fluorescence signal in standard FCS. For the forward scattered signal, it can be noted that the relative amplitudes of the negative spikes compared with the signal baseline are similar for the 780 nm latex beads (Figure 2 A) and the 730 nm silica beads (Figure 2 C), whereas they are clearly smaller for the 390 nm latex beads. This is in line with the expected behavior, that is, that the amplitudes reflect the volume of water that is displaced upon the particles passing through the detection volume (Figure 1). The absolute amplitudes of the spikes are different for the scattered light that was detected in the forward and backward directions, as further discussed in Sections 2.2 and 2.3.

2.2. Auto- and Cross-Correlation Analyses of the Forward and Backward CARS Signals

When the particles are smaller, or when the concentrations of the NPs are higher than in the measurements shown in Figure 2, meaning that on average several NPs are present in the detection volume at the same time, individual spikes can no longer be directly identified in the time traces of the CARS signals. In this case, the autocorrelation function (ACF) or cross-correlation function (CCF) of the fluctuations of the recorded CARS signals can provide information about the particle properties. For the negative spikes in the forward direction, we expect the ACF of the forward CARS signal to show similar features as the ACF curves recorded in iFCS.[7,8] For the positive spikes of the back-scattered CARS signal, the CCF of the backward and forward CARS signal should then display anti-correlative behavior, similar to the negative amplitude CCFs found in iFCCS experiments.[9]

The expected general behavior of the ACFs and CCFs was verified by experiments on polystyrene NPs with diameters of 390 and 780 nm, by applying auto- and cross-correlation analysis to the CARS signals recorded in the forward and backward direction (Figure 3). Figure 3 A shows how the amplitude of the forward signal ACFs, recorded from aqueous solution samples with 390 nm NPs at concentrations ranging from 2 to 50 pM, increases linearly with the NP concentration. This concentration dependence is well in line with that observed for ACFs recorded in iFCS experiments,[7,8] and the amplitudes are approximately given by Equation (1):

$$G(0)-1 = V_q^{\,2} \cdot N_p \qquad (1)$$

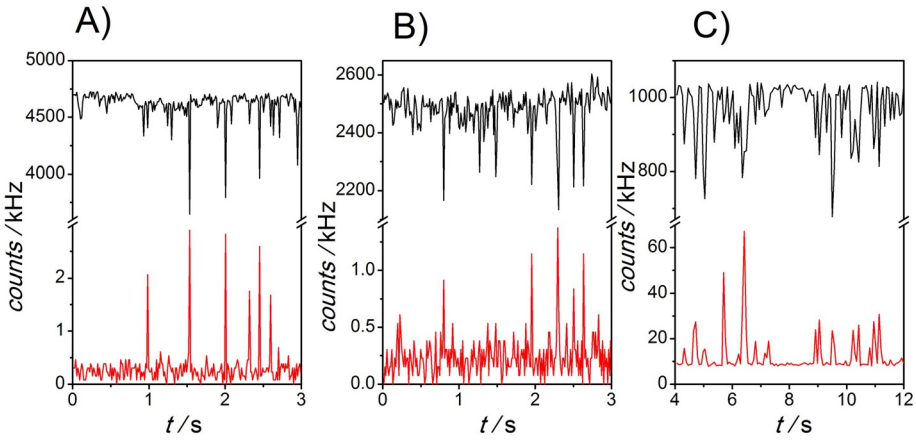

Figure 2. Traces of forward scattered (upper traces, black) and backward scattered (lower traces, red lines) signals from iCARS-CS measurements on NPs in aqueous solution. Dips in the forward signal are accompanied by positive spikes in the backward signal. A) latex beads 780 nm, B) latex beads 390 nm, C) silica beads 730 nm.

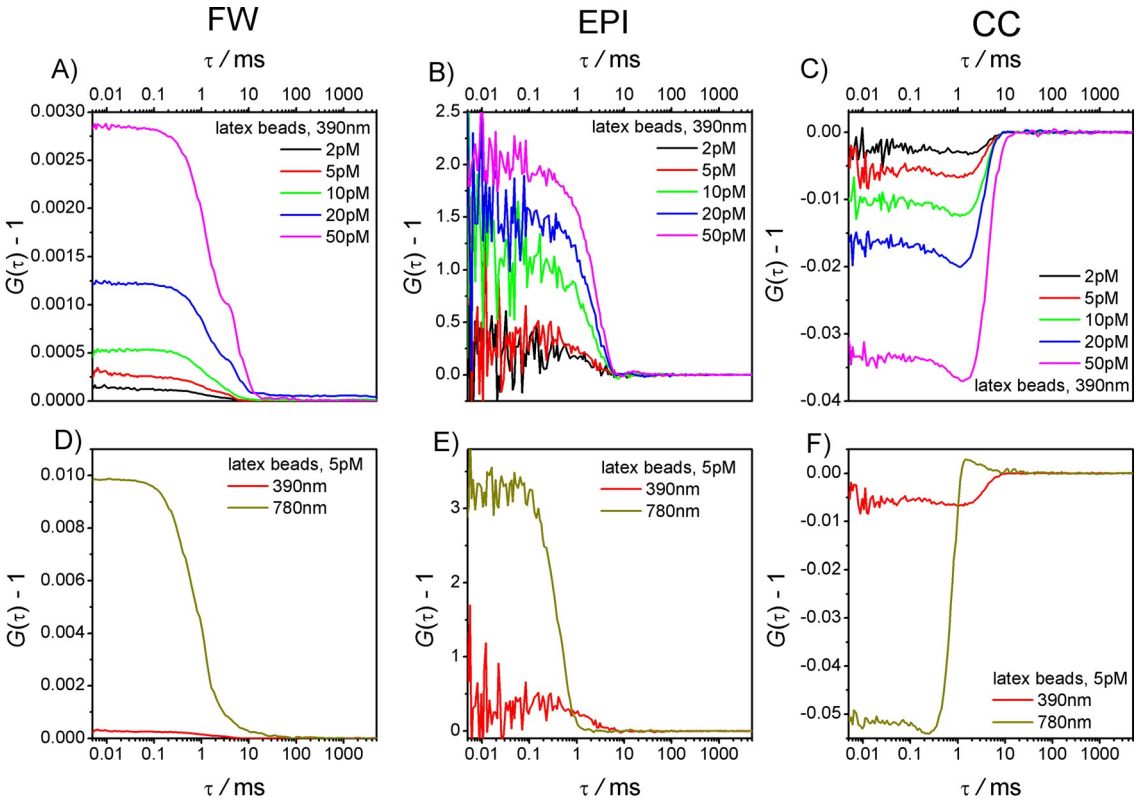

Figure 3. ACFs and CCFs of the CARS intensity detected in the forward (FW) and in the backward (EPI) direction from different samples of NPs in aqueous solution. A) FW ACFs from 390 nm NPs at different concentrations (2, 5, 10, 20, and 50 pM). B,C) EPI ACFs (B) and CCFs (C) from the same samples as in (A). D) FW ACFs from samples with 390 and with 780 nm NPs (5 pM). E) EPI ACFs for same measurements as in (D) and F) CCF from the same samples shown in (D) and (E).

Here, G is the ACF, $V_q = V_p/V_{dv}$, where V_p is the NP volume and V_{dv} is the detection volume, and N_p is the mean number of NPs in the detection volume. This approximation holds as long as $1/V_q \gg N_p$.[7] Given that the CARS traces detected in the forward direction are similar to the fluorescence traces recorded by iFCS, we expected to obtain similar features in the calculated ACFs. However, the signals are also different, for example, CARS is coherent, and fluorescence is not. We, therefore, also expected some differences between the calculated CARS ACFs and the iFCS curves, as discussed in Section 2.3.

For the backward signal from the same 390 nm NP samples, the ACF amplitudes also increased with the NP concentration, but not in a linear fashion (Figure 3B). The CCFs from the same sample series are shown in Figure 3C, and indeed show negative amplitudes. However, in contrast to iFCCS, for which the amplitudes of the CCFs are independent of the particle concentration (when crosstalk is negligible and the NP concentration is low, such that $1/V_q \gg N_p$),[9,11] the amplitudes of the CCFs of the forward and backward signals in iCARS-CS increased with higher NP concentrations. The observed deviation from linearity of the ACF amplitudes in Figure 3B, and the non-constant CCF amplitudes in Figure 3C can be attributed to the relatively large background signal present in the backward detection of the CARS signal. In Figure 3A, a slight bump at approximately 5 ms can be observed in the correlation curves recorded from the higher concentration (20 and 50 pM) bead samples; a possible reason for this is formation of bead agglomerates, followed by transient laser trapping of the agglomerates in the experiments.

Next, we investigated how the amplitudes of the ACFs and CCFs of the CARS intensity detected in the forward and backward directions depend on the volume of the NPs. Two aqueous samples containing equal concentrations of 390 and 780 nm diameter NPs were measured. For the ACF of the forward-detected CARS (Figure 3D), the difference in the amplitudes obtained from the 780 and 390 nm NP samples is close to that predicted by Equation (1); with the diameters of the NPs differing by a factor of two, the ACF amplitudes can be expected to differ by a factor of 64 ($V_p^2 \approx d^6$). The measured amplitudes in Figure 3D yield a diameter ratio of 2.14, compared with the real ratio of 2. For the corresponding ACFs of the backward-detected CARS (Figure 3E), the amplitudes differ by a factor of about eight. The lower amplitude difference in Figure 3E, as compared with Figure 3D, is likely because of the strong background signals present in the backward detection.

In general, the CARS signal in our experiments is predominantly emitted in the forward direction, with both the detected photon count levels and the spike amplitudes being two to four orders of magnitude higher than those in the backward direction (Figure 2). The forward signal, which is inevitably scattered and reflected also in the backward direction, can then strongly contribute to the strong background signal in

the backward direction, as well as to considerable crosstalk between the channels. Thus, it was difficult to reliably extract information from the ACF of the CARS intensity detected in the backward channel, and from the CCF of the intensities detected in the two channels, especially for small NPs and high NP concentrations.

2.3. NP-Size and -Concentration Dependence of the ACFs from the Forward CARS Signal

To determine in more detail how the amplitudes of the ACFs depend on the size and concentration of the NPs, iCARS-CS measurements of aqueous samples with different NP concentrations and with NPs of different sizes were systematically performed. Figure 4A depicts the amplitudes of the ACFs calculated from the forward CARS signal and recorded from samples with NPs with diameters ranging from 34 to 780 nm and at different concentrations. For particles with diameters of 200 nm or larger, ACF amplitudes were clearly resolved even for concentrations down to the picomolar range. For all NP sizes, a linear dependence of the amplitude to the concentration was seen, in accordance with Equation (1). In Figure 4A, the slopes of ACF amplitudes versus NP concentration was determined by linear regression. For each NP size the origin (0,0) was also included among the data points; this also allowed an estimate of the slopes for the smallest NPs (62 and 34 nm), for which only single data points were available. For these bead sizes, additional measurements at lower concentrations were not performed, due to low signal-to noise ratios.

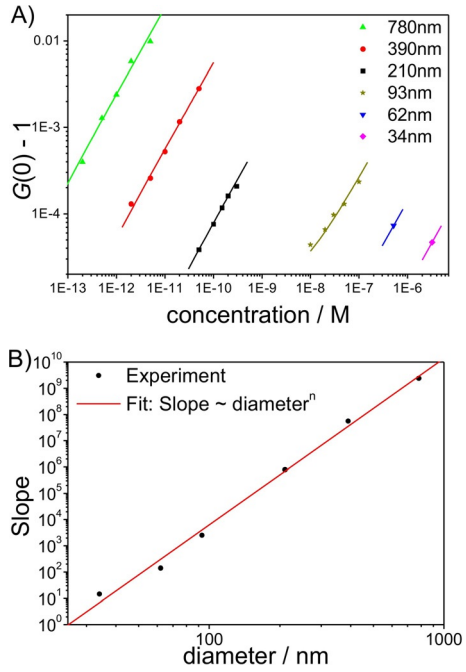

Figure 4. A) Amplitudes of ACFs recorded from the forward CARS signal, from aqueous samples with different NP diameters and concentrations. Solid lines: fits by linear regression. B) Slopes of the fitted lines in (A) for the different NP diameters. Solid line: fit by power dependence.

In Figure 4B, the slopes of the linear fits in Figure 4A are plotted versus the NP diameters and they follow a straight line on a log–log scale. This indicates that the slope-versus-diameter dependence can be described by a power function. The solid line shows the fit of such a power function (slope $\approx$ diameter^n) to the experimental points, which yields a value of $n = 6.3 +/- 0.3$ (slope $\approx V^{2.1+/-0.1}$). Accordingly, the amplitude of the forward-signal ACF scales with the sixth power of the NP diameter, or with the square of the NP volume. This is the same dependence as for iFCS [Eq. (1)], and thus, iCARS-CS shares the same ability as iFCS to determine NP sizes precisely. Following Equation (1), the amplitude of the ACF of the forward CARS signal can then be expressed in a similar form [Eq. (2)]:

$$G(0) - 1 = \alpha V_q^2 \cdot N_p \qquad (2)$$

where α is a constant factor accounting for differences in the generation of the dips in the (coherent) CARS signal in iCARS-CS and the dips in the (noncoherent) fluorescence signal in iFCS, and possible differences in V_{dv}. A derivation of $G(\tau)$ for iCARS-CS, referring to previous derivations for higher order FCS,[32] nonlinear[33] and CARS-based[20] correlation spectroscopy of particles, is given in the Supporting Information. A major difference in the derivation to those in Refs. [20,33,34] is that the particle concentration fluctuation term, δc, is replaced by $-<c>\delta C_p V_p$, that is, the negative fluctuation term of the volume displaced by the particles in the detection volume. Here, $<c>$ is the average concentration of water molecules (from which the signal is detected), and δC_p the NP concentration fluctuation term [see Equation (S16) in the Supporting Information].

2.4. Detection of Unlabeled Lipid Vesicles

To test the application of iCARS-CS beyond the characterization of NPs, the detection of μm-sized unilamellar lipid vesicles and smaller ones was also tested. As liposomes are filled with water, only their lipid bilayers contribute to an overall net displacement of water molecules upon their transit through the detection volume. The overall displaced water volume is, thus, much smaller than the whole liposome volume. In the experiments, as shown in Figure 5A, negative spikes could still be clearly observed in the forward CARS signal, as a result of the transit of lipid vesicles through the detection volume. The relatively prominent negative spikes are likely generated by the destruction of the coherence of the CARS signal, rather than by displacement of water molecules in the detection volume. ACFs of the CARS signal in the forward direction were acquired for liposomes ranging in size from 200 to 1000 nm (Figure 5B). As we couldn't control the concentration and size of the liposomes in our samples as precisely as for the NPs, the concentration and size dependence of the recorded ACFs (Figure 3 and 4) could not be accessed as accurately as for the NPs. However, clear trends in the dependencies on size (Figure 5B) and concentration for the ACFs from the forward CARS signal

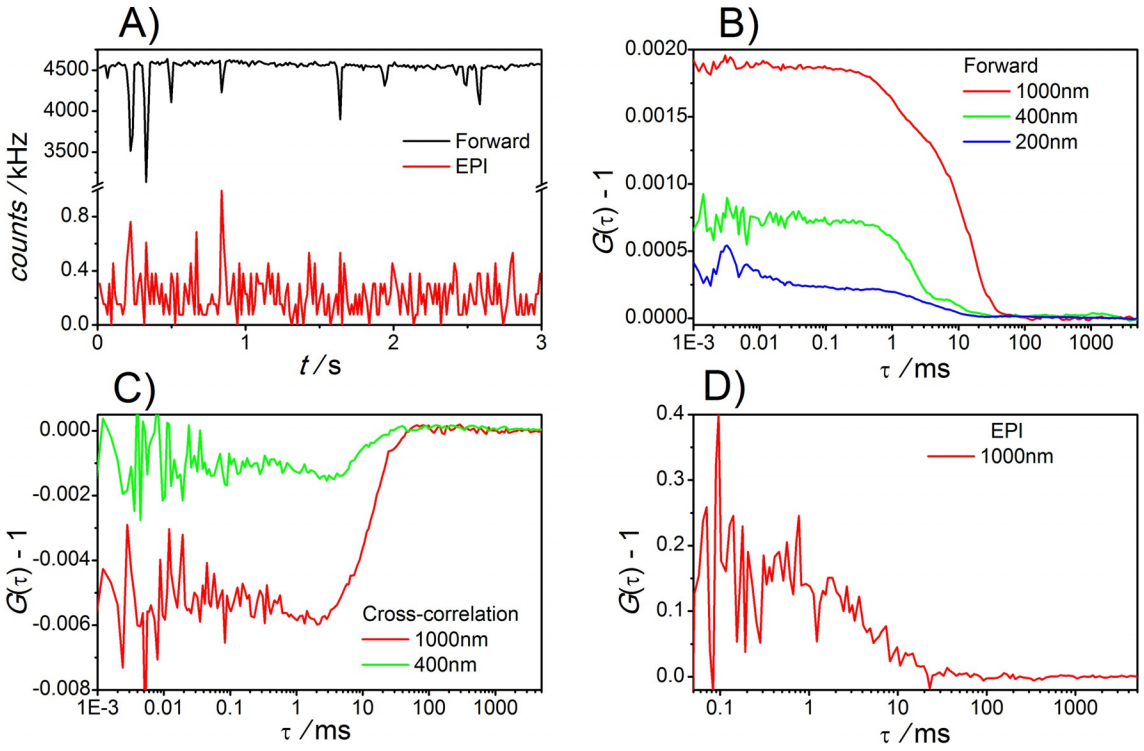

Figure 5. CARS intensity traces and correlation curves from liposome samples. A) CARS signals in the forward and EPI direction from a 1000 nm liposome sample. B) ACFs from the forward CARS signal, for liposomes with different diameters. C) CCFs of the forward and backward signals, recorded from samples with liposomes that are 400 and 1000 nm in diameter. D) ACF of the EPI signal from a sample with 1000 nm liposomes.

were observed. Also for EPI detection, spikes could be detected (Figure 5 A), although not as prominent, and CCFs with the forward CARS signal (Figure 5 C) and corresponding ACFs (Figure 5 D) could be generated, showing the same features as those recorded from the NPs.

3. Discussion

In this study, it was demonstrated that the CARS signal generated from solvent/medium molecules themselves can replace the fluorescence signal from a relatively highly concentrated fluorophore solution/medium, as used in iFCS. More specifically, it was shown how correlation analyses of a CARS signal from plain water molecules can provide size, concentration, and mobility information about particles and vesicles in aqueous solutions, with quite limited requirements on the signal strength per water molecule. The present approach is quite generally applicable, as in the absence of labels it can be used to determine the presence or movement of particles into and out of a confined detection volume by specifically registering the displacement of small volumes of water out of the detection volume by the particles.

In our experiments, the ACF of the forward CARS signal distinctly depended on the particle size and concentration, in a similar manner as in iFCS,[7,8] but offered fully label-free measurements. The amplitudes of the ACFs displayed a sixth power dependence on the diameters of the particles, which was used for sensitive size determinations down to tens of nanometers. However, as the amplitudes depend on both the particle size and concentration, they can only provide information about the concentration of the particles when the size is known, or vice versa.

Both parameters can in principle be resolved by also utilizing the backward CARS signal, through its ACF, or through the CCF of the forward and backward signals. A problem, however, is the scattering and reflection of the strong signal in the forward direction into the backward detection channel. We could significantly reduce the background signal in the backward channel by controlling polarization,[20,29] and by placing a pinhole in the back focal plane, although CARS microscopy is intrinsically confocal. Still, the reduction wasn't enough to be able to reliably use the backward signal for this purpose.

Another strategy to obtain information on both the particle size and concentration is to record the amplitude of the ACF of the forward-scattered CARS in two or more consecutive measurements (Figure 4), and by diluting the sample in a defined manner in between recordings. Alternatively, the decay times of the recorded ACFs can be exploited, which, like in FCS, should be proportional to the radius of the particles.[1,2] This approach was, however, complicated by the conflicting demands of signal strength and avoidance of optical-trapping effects.[34,35] Concerning the signal strength, the CARS signal is a nonlinear process, and ultrafast lasers are, thus, preferable light sources. For CARS microscopy, there is a trade-off between spectral resolution, providing chemical selectivity, and peak power, necessary to ensure sufficient signal levels. Use of femtosecond lasers yields high peak powers and signals, but typically also signals with spectral widths that are too broad to

resolve the molecular bands of interest. Instead, picosecond lasers have been found to offer more optimal pulse durations.[36] For iCARS-CS, the trade-off between spectral resolution and signal strength is a bit different. The CARS signal originates from the strongest Raman band (3100–3600 cm^{-1}) of the bulk water molecules. This band is broad, but still quite separate from most other biologically relevant bands.[36] The spectral resolution is therefore not so critical, and we can utilize a femtosecond laser as a light source, thereby reducing the average power needed for sufficient CARS signal levels. Still, with the Ti:Sapphire laser used in this study (fixed pulse repetition rate of 76 MHz, ≈130 fs long pulses), average powers in the mW range were required to achieve such levels. Exchange of momentum between the laser light and the particles then has to be considered.[34,35] The studied particles will then not undergo free diffusion and the correlation curves will be affected both in their shapes, amplitudes, and correlation times. As a solution to this problem, we used a flow cell[33] in our experiments. The flow practically eliminates the influence of the light force, but the correlation time will still not provide information about the diffusion time, but rather reflect the flow rate applied. Nevertheless, to demonstrate that the recorded ACFs can reflect the particle mobility, iCARS-CS measurements of 400 nm latex beads in water were performed under different flow rates (Figure S1), and the decay times of the ACFs were found to decrease with increasing flow rates. Apart from this, the mobility aspects were not further analyzed. However, for the future realization of iCARS-CS, using lasers with lower repetition rates by using, for example, pulse pickers, and/or shorter pulse durations,[37] reduced average powers and higher peak intensities could likely be obtained to generate sufficient CARS signals without light-force artifacts. Thereby, it should also be possible to analyze mobility aspects related to the diffusive properties of the particles in detail.

In this study, we present results utilizing the CARS signal from the most abundant biological medium—aqueous media and the water molecules themselves. CARS is the result of coherent nonlinear enhancement of radiation from an ensemble of coherently induced Raman modes in a large number of scatterers. As such, CARS is not suitable for single-molecule-microscopy applications[18,38,39].From a sensitivity point of view, it is thus beneficial to perform iCARS-CS based on a CARS signal that is coherently amplified by many scattering molecules in high concentrations, such as water molecules in aqueous solutions, rather than from CARS originating from individual molecules passing through the detection volume, as in CARS correlation spectroscopy.[17,25] The methodology is, however, not limited to aqueous samples. A general requirement for iCARS-CS is that a strong vibrational band can be identified; this band should be specific for molecules abundant in the sample medium, in other words, it should not be present in the dissolved particles to be studied. Apart from water, selective CARS signals can also be collected from a wide range of other media. As an alternative, one can also exploit isotope shifts to obtain vibrational bands of the medium that are not present in the dissolved particles to be studied. We proved the feasibility of iCARS-CS in ethanol and glycerin (Figure S2 in the Supporting Information) and also performed iCARS-CS measurements of NPs in heavy water (data not shown).

As the wavelength of CARS is shorter than that from the incoming laser light, cross-talk with one-photon excited fluorescence is negligible in CARS microscopy. However, with ultrashort laser excitation pulses, fluorescence may also be generated by nonlinear two-photon (or multiphoton) excitation (TPE). For autofluorescent samples, with a possible spectral overlap with the CARS wavelength, one can then tune the lasers to avoid TPE fluorescence. Alternatively, for cross-correlation analyses, it should also be possible to simultaneously generate a CARS signal from the medium, and a spectrally separated fluorescence signal from the dissolved particles generated by TPE.

In this study using iCARS-CS, the lowest measureable ACF amplitudes were of the order of 10^{-6}. This is at least an order of magnitude higher than those measureable by iFCS. A major reason for this is that the CARS signal is more unstable than the fluorescence signal. This is to a large extent because of the inherent nonlinearity of the CARS process, but also because the laser light generation is highly nonlinear. The laser system includes several nonlinear processes (second harmonic generation, Kerr lens mode-locking, optical parametric down-conversion), contributing to instabilities in the laser powers, in turn generating fluctuations and an inability to measure low ACF amplitudes. With more stable lasers[37] these fluctuations are reduced, lower amplitude ACFs can be measured, and thus, also samples with smaller beads and in lower concentrations. Using other detector types, such as photodiodes that can sustain more than six orders of magnitude higher CARS signals than the single photon counting modules used in this study, will also enhance the sensitivity. Furthermore, reduction of the detection volume, for example, by confinement of the detection to subwavelength gold film apertures as previously used in iFCS,[11] can provide another strategy to allow analysis of smaller NPs and even proteins.

For the same reason, the sensitivity will also be enhanced if measurements are performed on a 2D surface,[12] instead of in a 3D solution. Of particular biological interest is to perform 2D iCARS-CS measurements by generating and detecting a specific CARS signal from lipids, for example, phospholipids or cholesterol, in biological membranes. Protein clusters, diffusing in the bilayer and into the excitation focus area, will then displace a larger fraction of the signal-generating molecules than is possible in a 3D diffusion situation. Given that a distinct CARS signal can be generated from the lipids in the membrane, such measurements may allow 2D diffusing objects that are 20 nm in diameter or smaller to be analyzed and sized.[8]

Moreover, in contrast to techniques such as DLS, which do not rely on nonlinear signals, the nonlinear nature of the CARS process also inherently confines the detection volume, provides 3D sectioning and the basis for iCARS-CS as an imaging modality. By scanning, spatial in addition to temporal fluctuations can also be analyzed, of the water content in the detection volume or possibly of for example, the lipid content in a biological membrane area.

4. Conclusions

We presented proof-of-principle measurements by iCARS-CS to provide measurements of NPs and liposomes in the complete absence of labels, by monitoring a signal retrieved from the surrounding bulk water. The major limitations in the present experimental realization of iCARS-CS can be attributed to the laser source. However, given the strong development of laser technology, and with more stable lasers generating shorter pulses already being commercially available, issues regarding laser trapping and instabilities encountered in our iCARS-CS measurements could likely be overcome. This would allow iCARS-CS measurements of NPs/liposomes to be performed at much lower concentrations and for smaller particle sizes, and also diffusion information to be retrieved. In traditional forms of correlation spectroscopy, where the analyzed signal comes from the molecules/particles themselves rather than from the surrounding medium, the brightness of the signal retrieved from each molecule has to be strong. In contrast, iCARS-CS is based on a signal from the surrounding medium, and thus, strong molecular brightness is not required as long as the signal-generating medium molecules are abundant. For many different fluid media, it should be possible to identify distinct vibrational bands, which are not present in the dissolved particles to be studied, for molecules that are abundant in the sample medium. iCARS-CS should, thus, be applicable in media other than water.

Experimental Section

The experimental setup established for iCARS-CS is shown in Figure 6. A 779 nm beam from a Ti:Sapphire laser (Mira 900, Coherent, Inc) was split by a beam splitter, where 10% of the total power was used as a Stokes beam and directed at the sample. The rest of the beam was used to pump an optical parametric oscillator (OPO; PP Auto, A·P·E Angewandte Physik & Elektronik GmbH), and the second harmonic of the OPO was then used as the pump/probe beam in our experiments. For all experiments a pump/probe beam of 617 nm was used. As the Ti:Sapphire laser pumped the OPO, the Stokes and pump/probe laser beams were intrinsically synchronized, and a delay path in one of the optical branches allowed us to overlap the femtosecond pulses (approx. 130 fs full width at half maximum) in time/space along the direction of propagation. A dichroic mirror (640 nm LP, Chroma Technology) combined the two beams and a half-wave plate in the path of the Stokes beam allowed us to change the relative polarization of the two beams. A second dichroic mirror (535 nm SP, Semrock) reflected the laser beams to the objective (Olympus, UPlan Apo/IR 60x, 1.20NA, water immersion), focusing the beams into the sample. The focal detection volume [with $1/e^2$ dimensions of approximately (+/−20%) 220 nm (radial) and 1.0 μm (axial)] was located inside a flow cell (Micronit Microfluidics BV), through which the sample solution was passed with a flow speed 300–1000 $\mu m\,s^{-1}$ perpendicular to the optical axis. The generated signal in the backward (EPI) direction was collected by the same objective, transmitted through the dichroic mirror, passed through optical filters (520/40 nm Chroma Technology + 525/100 Chroma Technology), a polarizer, and a pinhole in a back focal plane, before being registered by an Avalanche photodiode (APD, PerkinElmer, SPCM-AQRH-14). The signal in the forward direction was collected by a second objective (Edmund Optics, Plan Apo, 20x, 0.42NA, working distance 20 mm), passed through filters (520/40 nm Chroma Technology +525/50 nm Semrock), blocking directly scattered light from the pump/probe and Stokes beams, and then a polarizer, before being focused onto the detection area of the APD (PerkinElmer, SPCM-AQRH-14). The polarizers in the detection branches allowed detection of the specific polarization. They were set to minimize background in the backward direction, and to reduce the nonresonant component in the forward direction.[20,29] Scattering and reflections of the signal generated in the forward direction led to an increased background in the EPI detection path, as the signal generated in the forward direction was significantly higher than in the backward direction. Although, CARS microscopy is intrinsically confocal, the pinhole in the backward direction was necessary to reduce the background. The lasers power was adjusted by neutral density filters.

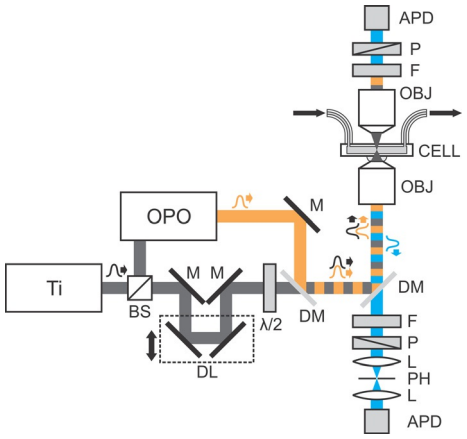

Figure 6. Schematic of the experimental setup for iCARS-CS: Ti–Ti: sapphire laser; OPO: optical parametric oscillator; BS: 90/10 Beam Splitter; M: Mirror; DL: delay line; λ/2: half-wave plate; DM: dichroic mirror; F: filter; P: polarizer; L: lens; PH: pinhole; APD: Avalanche photodiode; OBJ: objective; CELL: flow cell.

All beads in this study were acquired from commercial sources, the carboxyl latex beads (4% w/v, diameters of 26, 34, 62, 93, 210, 390, and 780 nm) from Invitrogen, and the silica beads from Bangs Laboratories (diameters of 730 and 490 nm). The beads were diluted in buffer, vortexed, and then added to the flow cell without prior sonication or other preparation steps. Liposomes were prepared from a chloroform solution of the 18:1 (Δ9-Cis) PC (DOPC) lipid (1,2-di-(9Z-octadecenoyl)-sn-glycero-3-phosphocholine, Avanti Polar Lipids, Inc., Alabaster, AL, USA). Following evaporation under nitrogen flow for 1 h, the lipids were dissolved in water. Then the lipid mixture was shaken for 1 h, by using a vortex mixer, to form multilaminar liposomes. Prior to extrusion through the final pore size (200–1000 nm), the suspension was disrupted by five freeze–thaw cycles. Then, the liposomes were extruded 21 times through a different polycarbonate membrane using an Avanti extruder (Avanti Polar Lipids) to produce unilamellar vesicles.

Acknowledgements

This study was supported by funds from the Swedish National Research Council (VR-NT, 2012-3045), Knut and Alice Wallenberg Foundation (KAW 2011.0218), and a visiting scholarship to M.D.R. from the Rajko and Maj Djermanovic Fund.

Keywords: CARS (coherent anti-Stokes Raman scattering) · FCS (fluorescence correlationspectroscopy) · label-free · microparticles · nanoparticles

[1] D. Magde, W. W. Webb, E. L. Elson, *Phys. Rev. Lett.* **1972**, *29*, 705 – 708.
[2] R. Rigler, Ü. Mets, J. Widengren, P. Kask, *Eur. Biophys. J.* **1993**, *22*, 169 – 175.
[3] R. Rigler, *Biochem. Biophys. Res. Commun.* **2010**, *396*, 170 – 175.
[4] E. L. Elson, *Biophys. J.* **2011**, *101*, 2855 – 2870.
[5] J. Ries, P. Schwille, *Bioessays* **2012**, *34*, 361 – 368.
[6] J. Widengren, in *Fluorescence Correlation Spectroscopy* (Eds: E L. Elson, R. Rigler), Springer, Berlin, Heidelberg, New York, **2001**, pp. 276 – 300.
[7] S. Wennmalm, L. Xu, P. Thyberg, J. Widengren, *Anal. Chem.* **2009**, *81*, 9209 – 9215.
[8] S. Wennmalm, J. Widengren, *Front. Biosci.* **2011**, 385 – 392.
[9] S. Wennmalm, J. Widengren, *Anal. Chem.* **2010**, *82*, 5646 – 5651.
[10] U. Meseth, R. Rigler, H. Vogel, *Biophys. J.* **1999**, *76*, 1619 – 1631.
[11] T. Sandén, R. Wyss, C. Santschi, G. Hassaïne, C. Deluz, O. J. F. Martin, S. Wennmalm, H. Vogel, *Nano Lett.* **2012**, *12*, 370 – 375.
[12] J. Bergstrand, D. Rönnlund, J. Widengren, S. Wennmalm, *Opt. Express* **2014**, *22*, 13073 – 13090.
[13] B. J. Berne, R. Pecora, in *Dynamic Light Scattering*, Wiley, New York, **1975**.
[14] C. Eggeling, J. Schaffer, C. A. M. Seidel, J. Korte, G. Brehm, S. Schneider, W. Schrof, *J. Phys. Chem. A* **2001**, *105*, 3673 – 3679.
[15] E. J. Bjerneld, Z. Földes-Papp, M. Käll, R. Rigler, *J. Phys. Chem. B* **2002**, *106*, 1213 – 1218.
[16] L. C. Tang, C. Q. Dong, J. C. Ren, *Talanta* **2010**, *81*, 1560 – 1567.
[17] J. I. Dadap, H. B. de Aguiar, S. Roke, *J. Chem. Phys.* **2009**, *130*, 214710.
[18] A. Tcherniak, S. Dominguez-Medina, W. S. Chang, P. Swangalap, L. S. Slaughter, C. F. Landes, S. Link, *J. Phys. Chem. C* **2011**, *115*, 15938 – 15949.
[19] T. Hellerer, A. Schiller, G. Jung, A. Zumbusch, *ChemPhysChem* **2002**, *3*, 630 – 633.
[20] J. Cheng, E. O. Potma, S. X. Xie, *J. Phys. Chem. A* **2002**, *106*, 8561 – 8568.
[21] P. M. R. Paulo, A. Gaiduk, F. Kulzer, S. F. G. Krens, H. P. Spaink, T. Schmidt, M. Orrit, *J. Phys. Chem. C* **2009**, *113*, 1145111457.
[22] S. Wennmalm, J. Widengren, *J. Am. Chem. Soc.* **2012**, *134*, 19516 – 19519.
[23] S. Broillet, A. Sato, S. Geissbuehler, C. Pache, A. Bouwens, T. Lasser, M. Leutenegger, *Opt. Express* **2014**, *22*, 782 – 802.
[24] D. E. Koppel, *Phys. Rev. A* **1974**, *10*, 1938 – 1945.
[25] G. Raposo, W. Stoorvogel, *J. Cell Biol.* **2013**, *200*, 373 – 383.
[26] N. Arraud, R. Linares, S. Tan, C. Gounou, J. M. Pasquet, S. Mornet, A. R. Brisson, *J. Thromb. Haemostasis* **2014**, *12*, 614 – 627.
[27] D. Robbins, A. E. Morelli, *Nat.Rev. Immunol.* **2014**, *14*, 195 – 208.
[28] C. D'Souza-Schorey, J. W. Clancy, *Genes Dev.* **2012**, *26*, 1287 – 1299.
[29] J. X. Cheng, A. Volkmer, X. S. Xie, *J. Opt. Soc. Am. B* **2002**, *19*, 1363 – 1375.
[30] A. Volkmer, J. X. Cheng, X. S. Xie, *Phys. Rev. Lett.* **2001**, *87*, 023901.
[31] M. Marrocco, *J. Phys. Chem. A* **2008**, *112*, 13458 – 13462.
[32] A. G. Palmer, N. L. Thompson, *Biophys. J.* **1987**, *52*, 257 – 270.
[33] M. Geissbuehler, L. Bonacina, V. Shcheslavskiy, N. L. Bocchio, S. Geissbuehler, M. Leutenegger, I. Märki, J. P. Wolf, T. Lasser, *Nano Lett.* **2012**, *12*, 1668 – 1672.
[34] A. Ashkin, *Phys. Rev. Lett.* **1970**, *24*, 156 – 159.
[35] J. W. Chan, H. Winhold, S. M. Lane, T. Huser, *IEEE J. Sel. Top. Quantum Electron.* **2005**, *11*, 858 – 863.
[36] C. L. Evans, X. S. Xie, *Annu. Rev. Anal. Chem.* **2008**, *1*, 883 – 909.
[37] H. Fattahi, H. G. Barros, M. Gorjan, T. Nubbemeyer, B. Alsaif, C. Y. Teisset, M. Schultze, S. Prinz, M. Haefner, M. Ueffing, A. Alismail, L. Vámos, A. Schwarz, O. Pronin, J. Brons, X. T. Geng, G. Arisholm, M. F. Ciappina, V. S. Yakovlev, D. E. Kim, A. M. Azzeer, N. Karpowicz, D. Sutter, Z. Major, T. Metzger, F. Krausz, *Optica* **2014**, *1*, 45 – 63.
[38] A. Volkmer, *J. Phys. D* **2005**, *38*, R59 – R81.
[39] M. Müller, A. Zumbusch, *ChemPhysChem* **2007**, *8*, 2156 – 2170.

Manuscript received: December 7, 2015
Accepted Article published: January 28, 2016
Final Article published: February 11, 2016

